
Signature-Kernel Based Evaluation Metrics for Robust Probabilistic and Tail-Event Forecasting

Benjamin R. Redhead¹ Thomas Lee¹ Peng Gu² Victor Elvira² Amos Storkey¹

Abstract

Probabilistic forecasting is increasingly critical across high-stakes domains, from finance and epidemiology to climate science. However, current evaluation frameworks lack a consensus metric and suffer from two critical flaws: they often assume independence across time steps or variables, and they demonstrably lack sensitivity to tail events, the very occurrences that are most pivotal in real-world decision-making. To address these limitations, we propose two kernel-based metrics: the signature maximum mean discrepancy (Sig-MMD) and our novel censored Sig-MMD (CSig-MMD). By leveraging the signature kernel, these metrics capture complex inter-variate and inter-temporal dependencies and remain robust to missing data. Furthermore, CSig-MMD introduces a censoring scheme that prioritizes a forecaster's capability to predict tail events while strictly maintaining properness, a vital property for a good scoring rule. These metrics enable a more reliable evaluation of direct multi-step forecasting, facilitating the development of more robust probabilistic algorithms.

1. Introduction

Probabilistic Forecasting is of growing importance to real-world applications in a diverse range of fields, such as finance, smart energy, medicine, meteorology, and seismology. Within these application areas, it is often crucial to be able to capture the tail distributions well, so as to anticipate rare but high-risk events. Despite this, modern evaluation metrics often focus on the overall estimation of a distribution, smoothing out or even ignoring tail performance by summing or averaging across time-steps. Furthermore, the current state of the art evaluation metrics such as energy

¹School of Informatics, University of Edinburgh, Edinburgh, UK ²School of Mathematics, University of Edinburgh, Edinburgh, UK. Correspondence to: Benjamin R. Redhead <b.r.l.redhead@sms.ed.ac.uk>.

Preprint. February 12, 2026.

score (ES) or continuous ranked probability score (CRPS) are insensitive to temporal structure, with CRPS also assuming variate independence. This demonstrates that current evaluation metrics are unfit for a correct and sensitive evaluation of a joint distribution produced by a forecasting model, and fail to assess tail-forecasting performance.

We propose to overcome these limitations via utilising signature kernel metrics allowing for an evaluation of the overall geometry of a series and capturing the joint-distribution utilising output samples from the forecaster. To do this we leverage the signature kernel MMD and show its efficacy on synthetic and real-world time-series forecasting. In addition, we propose a novel censored metric following the approach of (de Punder et al., 2025) to focus on tail-events, defined via a Mahalanobis distance. This allows our metrics to distinguish forecasters which learn a more accurate joint-distribution or model tails more effectively, using only samples of the ground-truth and learned distribution. The practical results of this can be seen in Fig. 1, which compares outputs from the forecasters which receive the best score on our proposed metrics, and those which receive the best score on standard metrics.

The key contributions established in this paper are:

- We provide improved evaluation metrics that significantly enhance our ability to identify problematic forecasts, and hence will aid the future development of improved forecasting methods
- We provide a novel censored evaluation metric which preserves properness and effectively measures tail forecasting performance.
- We utilise signature-kernel maximum mean discrepancy for evaluation of time-series forecasters and demonstrate its efficacy via synthetic and real-world experiments.

Altogether, this work shows the significant need for much improved metrics for probabilistic forecasting. It establishes new and highly effective metrics with good theoretical properties that still only require forecasters to have sampling capability rather than full joint density definition.

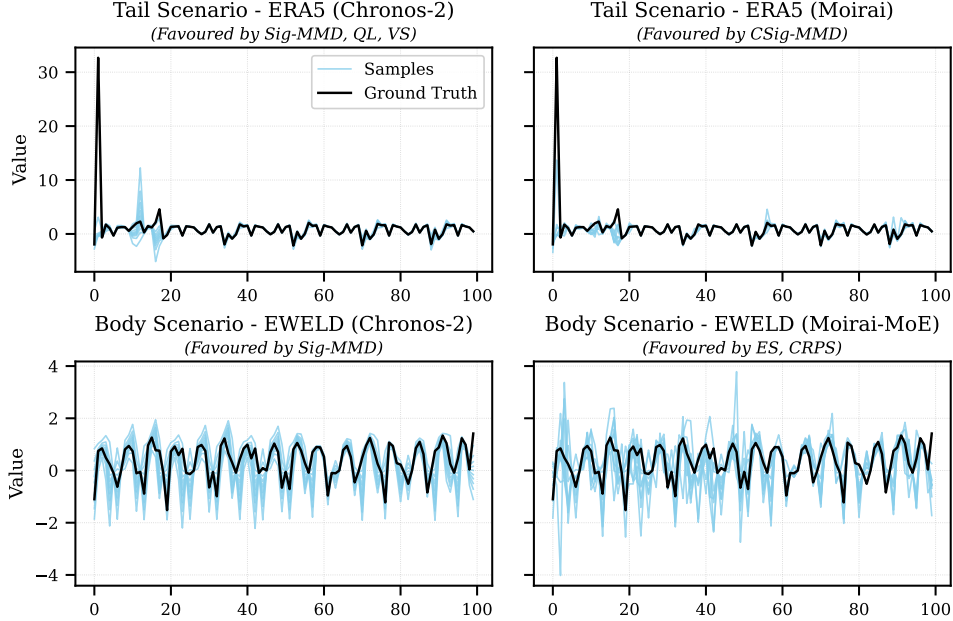


Figure 1. Comparison of forecast samples on Tail (Top, ERA5) and Body (Bottom, EWELD) scenarios. Top: Chronos-2, which receives the lowest score from Sig-MMD, QL, and VS, fails to predict the initial extreme spike, predicting phantom spikes later instead. In contrast, Moirai, which scores lowest on our censored metric (CSig-MMD), successfully captures the magnitude and timing of the initial tail event. Bottom: In the body scenario, Chronos-2 which scores lowest on Sig-MMD fits the series geometry closely with low noise. This contrasts with Moirai-MoE which scores lowest on CRPS and ES, and produces noisier samples that adhere less strictly to the ground truth scale. This highlights the efficacy of signature-based metrics in distinguishing shape and tail fidelity where standard metrics fail.

2. Related Work

Currently, when evaluating probabilistic time-series forecasters the primary metrics used are Quantile-Loss (Ansari et al., 2025; Shchur et al., 2025; Liu et al., 2025c;a; Kan et al., 2022), Continuous Ranked Probability Score (Baron et al., 2025; Dai et al., 2025; Aksu et al., 2024; Zhang et al., 2024; Liu et al., 2025c; Cortes et al., 2025; Rasul et al., 2024; Salinas et al., 2019; Kan et al., 2022; Liu et al., 2025b), Energy Score (Kan et al., 2022), or to measure variate correlations, Variogram Score (Baron et al., 2025). However, each of these metrics have their own issues which can lead to a flawed investigation of these probabilistic forecasters especially with regards to the accuracy of the forecast joint-distribution and the forecaster’s capability for risk aware prediction, we demonstrate this via synthetic experiments, shown later in Tab. 2 and Tab. 3. This is also theoretically validated for ES (Scheuerer & Hamill, 2015) and CRPS (Koochali et al., 2022). Due to similar issues with evaluation in spatio-temporal forecasting the usage of signature kernel maximum mean discrepancy originally proposed in (Chevyrev & Oberhauser, 2022) was adapted to spatio-temporal forecasting (Dodson & Dutta, 2025) however this work specifically focussed on the evaluation of this metric on weather data and with no analysis of how it measures tail forecasting performance. We establish the efficacy of signature kernel MMD in evaluating probabilistic forecasting

of multivariate time series, offering a thorough analysis of the theoretical benefits and an experimental evaluation on various synthetic and real-world data. Most importantly, we identify that Sig-MMD lacks the ability to prioritise forecasters which accurately capture the tails of a distribution and propose a novel censored metric to facilitate this. While a solution to tail forecasting evaluation has been proposed in the form of threshold weighted CRPS (Gneiting & Ranjan, 2011) it has been proven in (de Punder et al., 2025) this does not preserve properness and as it is based on CRPS will also inherit the same issues with regards to sensitivity of correlation structures.

Amongst all of these metrics, two stand out as the most popular for benchmarking probabilistic forecasters: CRPS and Quantile Loss. Yet despite this favour, it is known that these methods are calculated in a univariate manner for each component or time-step. This enforces an assumption of variate independence or a hierarchical forecasting assumption, and fails to adapt scoring for temporal dependence. This may be untrue in real-world data. The properties of each of these key metrics is displayed in Tab. 1 which discusses if the metrics are over a continuous time axis, assess multi-variate forecasts, account for time-dependency, maintain being proper when evaluated on finite samples, and are focussed on tail events. We also note we do not compare with metrics such as negative log likelihood, or tail-focussed

metrics derived from extreme value theory which require an explicit density to be provided as we make the problem formulation versatile for the forecaster by allowing it to output samples while still effectively capturing the ability to forecast tails and capture the joint distribution.

3. Preliminaries

3.1. Probabilistic Time-Series Forecasting

First, we define the problem of probabilistic time series forecasting, especially in the multivariate scenario. For a given set of variates $\mathbf{x}_{t_i} = x_{t_i,1}, x_{t_i,2}, \dots, x_{t_i,n}$ where $\mathbf{x}_{t_i} \in \mathbb{R}^N$ and $t_i \in \mathbb{R}$ and exogenous observations, which form part of the historical observation but are not forecast by our model, $\mathbf{o}_{t_i} = o_{t_i,1}, o_{t_i,2}, \dots, o_{t_i,m}$ where $\mathbf{o}_{t_i} \in \mathbb{R}^M$ forming a random field with index set $I = \{t_1, \dots, t_l\} \subset \mathbb{R}$ where $t_1 < t_2 < \dots < t_l$ the forecast is defined as

$$F(\mathbf{x}_{[t,t+l]} | X_{[1,t-1]}, O_{[1,t-1]}) = \quad (1)$$

$$p(\mathbf{x}_{t_{l+1}}, \mathbf{x}_{t_{l+2}}, \dots, \mathbf{x}_{t_{l+h}} | X_{[1,t-1]}, O_{[1,t-1]}). \quad (2)$$

That is, the forecast produces the joint-conditional pdf of the random field given the historical values and observations, on the forecast horizon index $I' = \{t_{l+1}, t_{l+2}, \dots, t_{l+h}\} \subset \mathbb{R}$. In practice, forecasters learn a distribution Q which is an estimation of the true distribution P learned from a finite amount of training samples.

3.2. Maximum Mean Discrepancy

In this subsection we define proper scoring rules, introduce maximum mean discrepancy, the theoretical underpinning of our proposed scoring rules, and discuss its properties.

Scoring rules: A score $S(Q, y)$ is *proper* if the expected score under the true distribution P is minimized by reporting $Q = P$:

$$\mathbb{E}_{y \sim P}[S(P, y)] \leq \mathbb{E}_{y \sim P}[S(Q, y)] \quad \forall Q \in \mathcal{P}.$$

Furthermore, a scoring rule is *strictly proper* if this minimum is unique, such that the equality holds if and only if $Q = P$:

$$\mathbb{E}_{y \sim P}[S(P, y)] = \mathbb{E}_{y \sim P}[S(Q, y)] \iff Q = P.$$

Maximum Mean Discrepancy (Gretton et al., 2012) is a proper scoring rule, and is strictly proper when utilizing a characteristic kernel. A kernel is defined as characteristic if it provides an injective mapping of probability measures into a Reproducing Kernel Hilbert Space (RKHS), thereby allowing for the unique representation and comparison of mean embeddings.

The Maximum Mean Discrepancy is formulated as the

Table 1. Comparison of scoring rules with regards to their properties. Quantile Loss only evaluates a function at the quantile points which is only relevant in univariate settings, CRPS is univariate, ES is an aggregate over time and loses sensitivity to multi-variate correlations as dimension increases, VS is aggregate over time, and due to the kernel trick both Sig-MMD and correspondingly CSig-MMD maintain propriety when using a Monte-Carlo estimate of the mean.

	Contin- uous Time	Multi- variate	Accounts for Time- Dep.	Proper Estima- tors	Focused on Tail Events
QL	✗	✗	✗	✗	✗
CRPS	✓	✗	✗	✗	✗
ES	✓	✓ [*]	✗	✗	✗
VS	✓	✓	✗	✗	✗
Sig (Ours)	✓	✓	✓	✓	✗
CSig (Ours)	✓	✓	✓	✓	✓

squared distance between kernel embeddings in the RKHS:

$$MMD^2(P, Q) = \|\mu_P - \mu_Q\|_{\mathcal{H}}^2,$$

where the kernel embedding $\mu_P \in \mathcal{H}$ is defined as

$$\mu_P := \mathbb{E}_{X \sim P}[k(X, \cdot)].$$

Here, k represents the chosen kernel function and \mathcal{H} is the RKHS forming the codomain of the kernel mapping.

One benefit of the MMD is that it does not require an explicit density function $p(x)$, is a proper scoring rule, and admits both biased and unbiased estimators that preserve properness (Zawadzki & Lahaie, 2015). This is necessary as we do not require forecasters to output a density, we only require samples output from the forecaster to compare with ground truth observations. Additionally, when using a characteristic kernel MMD does not just evaluate the forecast based on means but also on higher order moments embedded in a RKHS. This evaluation of higher order moments provides a more robust method to determine if two samples are from the same distribution.

3.3. Signature Kernel

The signature of a time series is a graded sequence of statistics that provides a path-based representation derived from the continuous interpolation of discrete data points. A defining property of the signature is its invariance to reparametrisation (Lyons & McLeod, 2025); it remains constant regardless of the sampling frequency or the speed at which the path is traversed, while remaining uniquely sensitive to the sequence order and the geometric profile of the trajectory. Furthermore, specific path augmentations, such as the inclusion of time and base-point coordinates (Morrill et al., 2021), can be applied to ensure the representation captures information regarding translation and temporal duration.

The signature of a continuous path, $x : [a \times b] \rightarrow \mathbb{R}^{2d}$ is then defined as:

$$S_{a,t}(x) = \prod_{n=0}^{\infty} S_{a,t}^n(x),$$

where components are defined as:

$$S_{a,t}^0(x) \equiv 1,$$

and for $n > 0$:

$$S_{a,t}^n(x) = \int_{a < t_1 < \dots < t_n < t} dx_{t_1} \otimes \dots \otimes dx_{t_n}.$$

As this is an infinite product of iterated integrals, it cannot be computed for Machine Learning usages in this current form, a common solution to this is using a truncated signature of K components. Despite not scaling in complexity with path length or number of samples, a key drawback of signatures is their scaling with regards to dimensionality of the data as the truncated signature scales exponentially with regards to variates.

Due to their inherent ability to compare sequential data of different length and size, signatures are well-suited to applications within kernel methods for sequential data (Kiraly & Oberhauser, 2019). To this end a kernel can be defined as the scalar product of the signature features as follows:

$$k : BV(\mathcal{H}) \times BV(\mathcal{H}) \rightarrow \mathbb{R}, \quad (3)$$

$$s.t. k(x.y) \rightarrow \langle S(x), S(y) \rangle_{T(\mathcal{H})}, \quad (4)$$

where $BV(\mathcal{H})$ is the space of paths of bounded variation taking values in the Hilbert space \mathcal{H} and $T(\mathcal{H})$ is the tensor algebra of said space. This kernel can be computed without truncation via the kernel trick where it is the solution to a Goursat PDE (Salvi et al., 2021). Using this kernel trick removes the exponential scaling with regards to dimension but has a linear scaling of $\mathcal{O}((L_X + L_Y) \cdot d)$ where L_X, L_Y are the lengths of the input paths of the signature kernel.

4. Proposed Metrics: Sig and CSig

In this section, we introduce signature kernel based evaluation metrics for probabilistic forecasting and risk-aware forecasting. The first of which is the Maximum Mean Discrepancy utilising the aforementioned Signature Kernel, and the second is a censored scoring rule designed to focus its evaluation on tail-events. These metrics allow for evaluation of the whole joint distribution output by a forecaster over the forecasting horizon, without assuming independence of time-steps or variates, facilitating a more robust evaluation.

4.1. Signature Maximum Mean Discrepancy (Sig-MMD)

To evaluate the joint distribution across the full range of predictions, we utilise the Signature Maximum Mean Discrepancy (Sig-MMD) (Chevyrev & Oberhauser, 2022). We

first take the Signature Kernel of the sequences lifted into a high-dimensional RKHS via a static kernel (Dodson & Dutta, 2025), the Radial Basis Function (RBF) kernel, giving

$$k_{sig} = \langle S(k_x), S(k_y) \rangle. \quad (5)$$

By first extracting signature features we map the complex temporal dependencies into a feature space. We then apply MMD to these features, effectively constructing a distance-sensitive metric that accounts for the geometric properties of the multivariate series. This can be formalized as follows:

$$\begin{aligned} d_{k_{sig}}^2(P, Q) &= \|\mu_P - \mu_Q\|_{\mathcal{H}_{sig}}^2 \\ &= \|\mathbb{E}_P[k_{sig}(X, \cdot)] - \mathbb{E}_Q[k_{sig}(Z, \cdot)]\|_{\mathcal{H}_{sig}}^2. \end{aligned} \quad (6)$$

To ensure this metric is sensitive to temporal shifts and translation, we perform time, base-point, and end-point augmentations giving the resulting sequence:

$$X = \{(\mathbf{0}, 0), (\mathbf{x}_1, t_1), \dots, (\mathbf{x}_h, t_h), (\mathbf{0}, t_{h+1})\}, \quad (7)$$

Where $\mathbf{0}, x_i \in \mathbb{R}^n$ and $t_i \in \mathbb{R}$. While Sig-MMD serves as a strictly proper scoring rule for the robust evaluation of the learned joint distribution, its global focus lacks sensitivity to low-probability events of extreme importance; namely, tail-events.

4.2. Metric Censoring (CSig-MMD)

We wish to construct a scoring rule that focusses on errors in the tail samples of the produced forecasts. However, it has been proven in (de Punder et al., 2025) that using a weighting alone for defining a metric on a specific focus region does not ensure the resulting metric is proper, thus we must use distribution censoring. Distribution censoring refers to the process of defining a region of interest, the censored region, and relocating probability mass outside this region to a set of one or more pivot points. For our censoring process, we first define a censored region to correspond to sequences that are in the tail of the joint distribution of a multi-variate time series (over the full time horizon). For this, we use a Mahalanobis distance:

$$d(\mathbf{x}, P) = \sqrt{(\mathbf{x} - \mu)^\top \Sigma^{-1} (\mathbf{x} - \mu)}, \quad (8)$$

where $\mathbf{x} \in \mathbb{R}^n$ is the point being evaluated, μ is the average over the data-points in P , the ground truth distribution, and Σ is a positive definite covariance matrix. For our specific case, to ensure the censoring and the censored metric all operate in the same metric space, defined on signatures, we first compute the truncated signatures, a signature which is

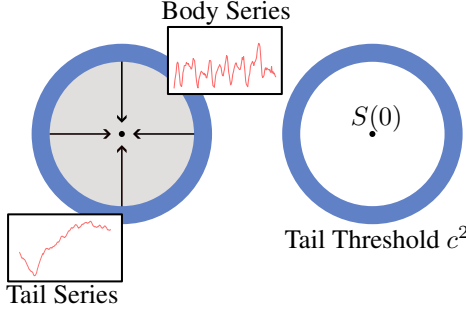


Figure 2. The censoring process redistributes the probability mass from the body of the distribution (grey) to the Signature of the zero-path, while preserving the probability mass inside the target region (blue) which represents the tails of the distribution.

reduced to only compute the first k terms, of the forecast and ground truth, denoted as $S[\mathbf{x}]$ for the truncation of $S(\mathbf{x})$, and then calculate the Mahalanobis distance as follows:

$$d(S[\mathbf{x}], P_s) = \sqrt{(S[\mathbf{x}] - \mu_s)^\top \Sigma_s^{-1} (S[\mathbf{x}] - \mu_s)}. \quad (9)$$

Following this, we define a soft weight function $w(\mathbf{x})$ using a generalized logistic function centred at the threshold c^2 , which corresponds to the $1 - \alpha$ quantile of the Mahalanobis distances of the truncated training signatures:

$$w(\mathbf{x}) = \frac{1}{1 + \exp(-\beta(d(S[\mathbf{x}], P_s) - c^2))}, \quad (10)$$

where β represents the steepness of the censoring boundary. This weighting identifies the region of interest A as the high-distance tail of the distribution, such that $w(\mathbf{x}) \rightarrow 1$ as the distance increases.

We then relocate the probability mass of the out-of-focus region to a pivotal point as illustrated in Fig. 2, for which we choose the zero-path $\mathbf{0} \in \mathbb{R}^{D+1}$. The zero-path is chosen as we utilise normalised paths inside this metric for stability and thus a natural pivot is the zero-path, the mean-path could also be used as it is certain that the mean path will not fall into the censored region for tail-event focused censoring. The censored distribution P^b is thus constructed such that its expectation for any function f is:

$$\mathbb{E}_{P^b}[f(X)] = \mathbb{E}_P[w(\mathbf{x})f(X) + (1 - w(\mathbf{x}))f(\mathbf{0})]. \quad (11)$$

By substituting these censored expectations into Eq. (6), we arrive at the Censored Signature Maximum Mean Discrepancy (CSig-MMD):

$$\begin{aligned} d_{k_{sig},b}^2(P, Q) &= \|\mu_{P^b} - \mu_{Q^b}\|_{\mathcal{H}_{sig}}^2 \\ &= \left\| \mathbb{E}_P[w(\mathbf{x})k_{sig}(X, \cdot) + (1 - w(\mathbf{x}))k_{sig}(\mathbf{0}, \cdot)] \right. \\ &\quad \left. - \mathbb{E}_Q[w(Y)k_{sig}(Y, \cdot) + (1 - w(Y))k_{sig}(\mathbf{0}, \cdot)] \right\|_{\mathcal{H}_{sig}}^2. \end{aligned} \quad (12)$$

Each term is expanded via Monte Carlo sampling to include the interactions between the weighted sample paths and the pivotal zero-path. This construction ensures that the metric is sensitive to discrepancies specifically within the tail behaviour, as any differences in the out-of-focus region are nullified by their shared relocation to the pivot.

To ensure sensitivity to timescale and translations, sequences are augmented as in Eq. (7). This results in a metric that captures complex dependencies in the joint distribution without assuming independence across variates or time-steps, while the censoring transformation ensures the evaluation is specifically focused on the performance of probabilistic forecasters on tail-events.

Proposition 4.1. *As k_{sig} is a characteristic signature kernel, let $w(x)$ be a measurable weighting function defining a censored distribution as in Eq. (11). Then censored Sig-MMD remains strictly proper. For any method defining the censored region such that it induces a fixed measurable partition of the sample space then the choice of censoring method does not effect the properness of the metric.*

Prop. 4.1 is proven in relation to any strictly proper scoring rule in (de Punder et al., 2025) as long as the censored distribution is constructed via correctly reallocating probability mass from outside the censored region to these pivotal points. We discuss why our specific implementation choices still satisfy this requirement in Sec. 5.1.

5. Experiments

5.1. Implementation Details

To implement our Mahalanobis distance and tail detection we had to use truncated signatures to ensure Σ_s and μ_s were well-defined. Additionally, to ensure the robustness of our Mahalanobis distance in detection of tails we utilised the Minimum Covariance Determinant (MCD) (Hubert et al., 2018) ensuring the covariance is defined so as to cover a proportion α of the data-points, in the case of the following experiments we set α to 80%. This ensures that tail-events inside the training-data do not over-inflate the covariance matrix and mean, ensuring our Mahalanobis Distance is effective at detecting outlier Signatures as tail-events. Additionally, to ensure computational efficiency when calculating the MCD on the whole of the training data, if the dataset exceeds a certain number of variates PCA is used to reduce the number of variates while maintaining the ability to explain variance greater than α . As these decisions only affect the censoring region and are all applied uniformly across all experimental scenarios they do not effect the metric properness discussed in Prop. 4.1. All experiments were conducted on a single A100 GPU with no change to hyper-parameters aside from censoring quantile as described in Sec. 5.3.1.

Table 2. Dependency Experiment: F_1 the forecaster outputs samples from the ground truth distribution, F_2 the forecaster outputs samples from the ground truth without temporal correlations, F_3 the forecaster outputs samples from the ground truth without spatial and temporal correlations, and F_4 the forecaster outputs samples from the ground truth with Bernoulli arrival jumps. This table shows that CRPS, ES, and VS are not proper when evaluated on samples and that these metrics and QL do not properly evaluate spatial and temporal correlations, whereas our proposed signature kernel based metrics capture these correlations effectively.

F	QL	CRPS	ES	VS	Sig	CSig
F_1	0.8184	0.5550	1.4384	3.8366	0.000733	0.000051
F_2	0.8191	0.5544	1.4367	3.8288	0.009174	0.000078
F_3	0.8190	0.5537	1.4602	4.0103	0.010376	0.000082
F_4	1.6723	1.1247	4.1421	3.8419	0.002757	0.000239

5.2. Synthetic Distribution Experiments

To validate the efficacy of SigMMD and CSig-MMD at recognising dependency structure and tail-forecasting capability we run two experiments on synthetic Gaussian Process data:

1. Dependency sensitivity tests, evaluating state-of-the-art methods against Sig-MMD and CSig-MMD at capturing inter-temporal and inter-variate dependencies in a forecast distribution
2. Focus capability tests comparing the ranking of Sig-MMD and CSig-MMD on forecasts where the errors are localised to the tails or the core distribution

For the dependency sensitivity experiment we set up a ground truth distribution, G , which is a Gaussian Process with 0 mean and a covariance matrix constructed as the Kronecker product of a temporal kernel and spatial covariance matrix:

$$K = K_t \otimes \Sigma_s,$$

where K_t is the RBF Kernel and Σ_s is a correlation matrix defined by sampling a matrix A from a standard normal distribution then normalising AA^T to provide a positive semi-definite matrix with diagonals of 1. Then four forecasts were constructed, F_1 , is identical to the ground truth, F_2 samples from $N(\mathbf{0}, \Sigma_s)$ preserving the spatial correlations but removing the time dependencies, F_3 , samples from $N(\mathbf{0}, \text{diag}(\Sigma_s))$ thus removing temporal and spatial dependencies, and F_4 , a jump-diffusion process where the base state is sampled from the ground-truth $\mathcal{N}(\mathbf{0}, K)$, augmented by additive jumps $\mathbf{J} = \mathbf{m} \odot \boldsymbol{\xi}$. Here, \mathbf{m} is a binary mask with entries $m_i \sim \text{Bernoulli}(p)$ representing jump arrivals, and $\boldsymbol{\xi} \sim \mathcal{N}(\mathbf{0}, \sigma_j^2 \mathbf{I})$ represents the jump magnitudes.

The results of the dependency experiments as shown in Tab. 2 show that ES, CRPS, and QL all fail to take into account the dependency structure of output forecasts, with

Table 3. Focus Experiment: F_1 the forecaster outputs the ground truth, F_2 paths from the body of the distribution have harmonic noise added, F_3 the forecaster samples from a t-distribution, F_4 the forecaster samples from a uniform distribution. This table shows that aside from CSig each metric gives a lower score to the forecaster which under represents tails compared to the one with a noisy body, whereas CSig focuses on tail prediction capability identifying the changes in tails as the worst outcomes.

F	QL	CRPS	ES	VS	Sig	CSig
F_1	0.0000	0.0000	0.0000	0.0000	0.000000	0.000000
F_2	1.0533	0.7022	1.7561	10.4096	0.158023	0.000000
F_3	0.8392	0.5780	1.6149	5.6161	0.229519	0.000203
F_4	0.7796	0.5638	1.4878	3.5802	0.058396	0.000153

these metrics either maintaining a similar score, or improving on F_2 and F_3 where we have removed the time and variate dependencies from the forecast distribution Q . Contrary to this, notice that the two proposed Signature based metrics are sensitive to these shifts, increasing for forecasts F_2 and F_3 . Due to the similarity in the overall shape of the forecast under the jump diffusion process F_4 performs better on the Signature-MMD metric than the two forecasts which have incorrect dependency structures, however as these jumps cause a greater number of tail samples where there are none in the ground truth the censored metric also significantly increases for F_4 . The results of these dependency experiments motivate a further analysis of the ability of current metrics to capture tail-forecasting performance, we do this via a set of synthetic focus experiments. These focus experiments have a ground truth Gaussian Process with 0 mean using the standard constant-RBF Kernel for the covariance kernel. We then test the metric at evaluating 4 forecasts: F_1 A forecast sampled from the ground truth, F_2 a forecast sampled from the ground truth however the maximum absolute value of a path is calculated and if it is below 2 standard deviations from the maximum absolute value of the mean path, this path is set to sinusoidal noise, presenting noised normal samples but tails from the ground truth distribution, F_3 is a t-distribution mixture with 2.1 degrees of freedom presenting wider tails than the ground-truth, and F_4 is a uniform distribution from $-\sqrt{3}$ to $\sqrt{3}$ to represent a forecast that misses the tails of the distribution.

The results of the focus experiments as shown in Tab. 3 clearly demonstrate the ability of the censored metric to evaluate tail forecasting accuracy effectively, where all other metrics have significant increase for forecasts F_2 , F_3 , F_4 , making which is preferable for tail-event forecasting indistinguishable, our proposed CSig-MMD only increases for F_3 and F_4 where the tail forecasts are inaccurate effectively demonstrating the metric's ability to identify and favour risk-aware forecasters.

Table 4. Aggregated Benchmarking Results (Wins/Ties/Losses). Blue indicates Wins (lowest score), Black indicates Ties (within 1% of lowest), and Red indicates Losses. This demonstrates the difference in ranking for CSig compared to other metrics, validating that it can provide unique insights into forecaster performance.

Model	QL	CRPS	ES	VS	Sig	CSig
DLinear	2, 0, 7	1, 0, 8	2, 1, 6	2, 0, 7	2, 0, 7	3, 0, 6
NLinear	1, 1, 7	2, 0, 7	3, 1, 5	0, 2, 7	1, 2, 6	2, 0, 7
PatchTST	2, 1, 6	2, 1, 6	2, 1, 6	4, 0, 5	3, 1, 5	2, 0, 7
iTransformer	1, 0, 8	0, 0, 9	0, 1, 8	0, 1, 8	0, 0, 9	1, 1, 7
TimesNet	0, 1, 8	1, 0, 8	1, 0, 8	1, 0, 8	1, 1, 7	0, 1, 8
N-HiTS	3, 4, 2	3, 0, 6	1, 2, 6	1, 0, 8	2, 1, 6	1, 2, 6
NSTransformer	0, 1, 8	0, 0, 9	0, 0, 9	1, 0, 8	0, 0, 9	0, 0, 9
Naive Seasonal	0, 0, 9	0, 0, 9	0, 0, 9	0, 0, 9	0, 0, 9	0, 0, 9

5.3. Learned Forecasters

5.3.1. DATASETS

Here we evaluate on the popular datasets used in TSLib (Wang et al., 2025), however due to the exponential scaling with variate size discussed in Sec. 3.3 we omit experiments on ECL and Traffic. Hence, evaluation occurs on *ETT*, *Weather*, *Exchange*, and *Illness*. Due to the characteristics of ETTh2, ETTm2 and Weather, the test set is relatively stable and lacking in tails, for this reason the usual Mahalanobis threshold of the 0.95 quantile is reduced to 0.8.

To further demonstrate the key use of our metric in tail forecasting scenarios we evaluate on two datasets containing extreme weather. First, we test on a modified version of *EWELD* (Liu et al., 2023). This modified version has 19 variates and is a combination of the weather series from all three key locations discussed in *EWELD*. Second, we use a dataset sourced from the Copernicus ERA5 (Copernicus Climate Change Service (C3S), 2026) Land time series data with a latitude of 37.6° and longitude of 127.0° corresponding to Seoul, South Korea and we take hourly weather data from 01-01-2000 to 31-12-2025, this dataset has 18 variates as listed in Appendix E.

5.3.2. FORECASTER RESULTS ANALYSIS

We compare learned models on each dataset and record wins (where the model scores lowest on the specific metric), losses, and ties (where for a given metric two models are within 1%). This is compared on DLinear, NLinear (Zeng et al., 2023), PatchTST (Nie et al., 2023), iTransformer (Liu et al., 2024), TimesNet (Wu et al., 2023), N-HiTS (Challu et al., 2023), Non-Stationary (NS) Transformer (Liu et al., 2022), and a Naive Seasonal Median. For each dataset we use an input sequence length of 96 and evaluate on a prediction window of 96 time-steps, with the exception of *Illness* which uses an input sequence length of 36 and a prediction length of 24.

Table 5. Aggregated Benchmarking Results for Foundation Models (Wins/Ties/Losses). Blue indicates Wins (lowest score), Black indicates Ties (within 1% of lowest), and Red indicates Losses. This shows the sharp distinction between CSig and other metrics, and validates the additional insight gained from evaluating foundation model forecasters with CSig.

Model	QL	CRPS	ES	VS	Sig	CSig
Chronos-2	9, 0, 0	2, 0, 7	2, 0, 7	9, 0, 0	9, 0, 0	4, 0, 5
Moirai	0, 0, 9	2, 0, 7	1, 1, 7	0, 0, 9	0, 0, 9	2, 2, 5
MoiraiMoE	0, 0, 9	5, 1, 3	6, 0, 3	0, 0, 9	0, 0, 9	3, 1, 5

To get these point-forecaster architectures to produce multivariate probabilistic forecasts we utilise a quantile regression head, and train them on each dataset via a quantile loss objective. As in (Shchur et al., 2023) we utilise win-rate to evaluate learned forecasters, the results of which can be seen in Tab. 4 with full results for each dataset available in Appendix A.

These results demonstrate that when adapted for the probabilistic forecasting task, the performance gap between state-of-the-art transformer-based forecasters and simple MLP or Linear architectures is significantly reduced. Notably, regarding tail forecasting, Linear models demonstrate a distinct competitive edge, outperforming complex architectures on metrics like CSig-MMD. This is likely attributable to the larger parameter counts in transformer-based models, which may encourage over-fitting to the body of the distribution at the expense of tail fidelity.

Additionally, while PatchTST demonstrates robust capabilities on larger datasets such as ETT, likely due to its patching mechanism effectively capturing hierarchical temporal relationships, it appears prone to the same over-fitting as other transformers on smaller datasets like *Illness* and *Exchange*, where simpler models dominate. Finally, while N-HiTS performs strongly on holistic distribution metrics like CRPS, its comparative underperformance on our tail-specific CSig-MMD reinforces the observation that increased model complexity can yield diminishing returns for extreme quantile estimation.

5.4. Zero-shot Foundation Models

5.4.1. BENCHMARK RESULT ANALYSIS

Here we evaluate the performance of foundation models on zero-shot forecasting in the datasets mentioned in Sec. 5.3.1. To the best of our knowledge there are only three foundation models which fulfil our necessary criteria of being multivariate, outputting probabilistic forecasts, and being open-source. The overall evaluation results of these forecasters can be seen in Tab. 5. These results show that for metrics which are sensitive to inter-variate correlations such as variogram score and Sig-MMD, Chronos-2 (Ansari et al.,

2025) outperforms its competitors. This is likely because Chronos-2 handles inter-variate dependencies via a specialized group-attention mechanism, whereas Moirai (Woo et al., 2024) and Moirai-MoE (Liu et al., 2025b) handle multivariate scenarios via flattening them into a single sequence and applying attention over the concatenated token stream. Contrary to this, Moirai-MoE and Moirai rival Chronos-2 on metrics shown to be insensitive to variate correlations such as CRPS and ES. This links directly to the findings of our synthetic experiments where it was shown CRPS and ES can give a lower score even when the forecast removes correlations.

5.4.2. TAIL FORECASTING ANALYSIS

For tail forecasting it is interesting to see that the performance balance shifts. While Chronos-2 is still the overall winner with optimum performance across our benchmark datasets, it fails to capture the tails in extreme weather data compared to Moirai. This is likely due to the differences in their output heads. Chronos-2 employs a quantile regression head, which is trained to predict a discrete set of fixed quantiles. While this is distribution-free, it effectively imposes a ceiling on the model’s ability to extrapolate beyond the highest trained quantile. In contrast, Moirai uses a parametric output head, which imposes a continuous probability density function over the output. This parametric assumption allows Moirai to extrapolate the shape of the distribution into the extreme tails, giving it an advantage in modelling the tail behaviour characteristic of extreme weather events.

This can be confirmed by looking at the results in Appendix. B across metrics on EWELD in Tab. 22 and ERA5 in Tab. 23. These results clearly show that despite capturing body correlations more accurately, as demonstrated by the lower QL, VS, and Sig-MMD, Chronos-2 receives the worst score on CSig in both extreme weather tasks, demonstrating a key drawback of their chosen quantile regression output.

5.5. Ablation Study

To demonstrate the convergence behaviour of our censored Sig-MMD we conduct an ablation examining the score as the censoring quantile decreases. The results of this study are visualised in Fig. 3 which shows that when the censoring quantile is low, causing all events to register as tails, the metrics converge, however as the censoring quantile increases the scores diverge. This also highlights a key point about censored metrics, due to the relocation of a proportion of the probability mass the magnitude of the censored metric is lower than that of the uncensored one when the regions are properly calibrated. Alongside this we conduct ablations, in Appendix. C, on various hypothesis testing scenarios to find the combinations of dimension and number of samples where our methods have high statistical power as discussed

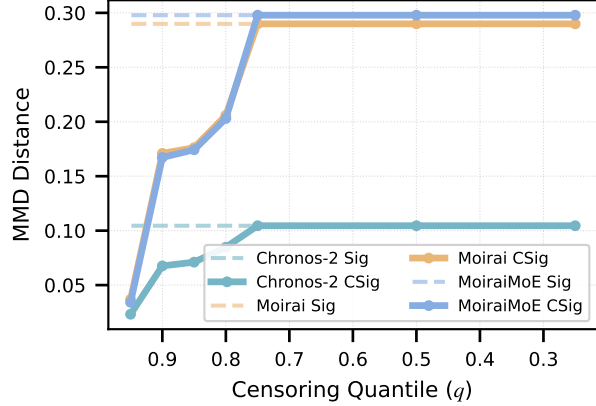


Figure 3. This figure displays how the score from CSig-MMD varies with censoring quantile on the Exchange dataset. This figure shows as censoring quantile is reduced more points fall into the tail region and as the tail region converges to the whole set of outcomes CSig-MMD converges to Sig-MMD.

in (Marcotte et al., 2023) and an ablation on Kernel type in Appendix. D.

6. Conclusions

Conclusions. This work encourages the use of signature kernel based metrics for the evaluation of probabilistic forecasting and shows the benefits of these metrics on synthetic and real-world experiments. Additionally, this work proposes a novel censored metric that can assess a forecaster’s ability to produce samples from the tail of a distribution accurately. This has been shown to provide novel insights into the features of the architecture of foundation model forecasters which could be missed by other metrics. The combination of these contributions facilitates an advancement in the capabilities of probabilistic forecasters especially with regards to tasks of pivotal importance such as risk-aware forecasting and multivariate forecasting.

Limitations and Future Work. Although the proposed metrics use of signatures allows them to effectively capture the joint-distribution implied by a forecaster, the usage of truncated signatures to calculate the Mahalanobis distance for censoring restricts the application of this metric to higher-dimensional scenarios. To fix this future work could include new censoring methods utilising the signature kernel which can then scale linearly with dimension, or can look at more efficient ways to compute signatures. Additionally, we hope our work motivates a shift away from CRPS for assessing the capabilities of probabilistic forecasters and the development of more capable forecasting models. Finally, this study proposed these metrics to evaluate the capabilities of a forecaster and did not assess their gradient behaviour and if they could be used as loss functions, leaving a gap for future research in the effects of training probabilistic forecasters on these metrics.

Impact Statement

This paper presents work whose goal is to advance the field of Machine Learning. There are many potential societal consequences of our work, none which we feel must be specifically highlighted here.

References

Aksu, T., Woo, G., Liu, J., Liu, X., Liu, C., Savarese, S., Xiong, C., and Sahoo, D. GIFT-Eval: A Benchmark For General Time Series Forecasting Model Evaluation. arXiv preprint arXiv:2410.10393 <http://arxiv.org/abs/2410.10393>, 2024.

Ansari, A. F., Shchur, O., Küken, J., Auer, A., Han, B., Mercado, P., Rangapuram, S. S., Shen, H., Stella, L., Zhang, X., Goswami, M., Kapoor, S., Maddix, D. C., Guerron, P., Hu, T., Yin, J., Erickson, N., Desai, P. M., Wang, H., Rangwala, H., Karypis, G., Wang, Y., and Bohlke-Schneider, M. Chronos-2: From Univariate to Universal Forecasting. arXiv preprint arXiv:2510.15821 <http://arxiv.org/abs/2510.15821>, 2025.

Baron, E., Oreshkin, B. N., Ma, R., Zhang, H., Torkkola, K., Mahoney, M. W., Wilson, A. G., and Konstantinova, T. Efficiently Generating Correlated Sample Paths from Multi-step Time Series Foundation Models. In *Proceedings of the Workshop on Recent Advances in Time Series Foundation Models: Have We Reached the 'BERT Moment'?*, 2025.

Challu, C., Olivares, K. G., Oreshkin, B. N., Ramirez, F. G., Canseco, M. M., and Dubrawski, A. NHITS: Neural Hierarchical Interpolation for Time Series Forecasting. In *Proceedings of the Thirty-Seventh AAAI Conference on Artificial Intelligence*, 2023.

Chevyrev, I. and Oberhauser, H. Signature Moments to Characterize Laws of Stochastic Processes. *Journal of Machine Learning Research*, 23(176):1–42, 2022.

Copernicus Climate Change Service (C3S). ERA5 Land hourly time-series data on single levels from 1950 to present. Climate Data Store (CDS) <https://cds.climate.copernicus.eu/datasets/reanalysis-era5-land-timeseries>, 2026. Accessed: 2026-01-25.

Cortes, A., Rehm, R., and Letzelter, V. Winner-takes-all for Multivariate Probabilistic Time Series Forecasting. In *Proceedings of the Forty-second International Conference on Machine Learning*, 2025.

Dai, X., Xu, Z., Cai, W., and Xu, Q. From Samples to Scenarios: A New Paradigm for Probabilistic Forecasting. arXiv preprint arXiv:2509.19975 <http://arxiv.org/abs/2509.19975>, 2025.

de Punder, R. F. A., Diks, C. G. H., Laeven, R. J. A., and van Dijk, D. J. C. Localizing Strictly Proper Scoring Rules*. *Journal of the American Statistical Association*, pp. 1–24, 2025.

Dodson, A. and Dutta, R. Signature Kernel Scoring Rule as Spatio-Temporal Diagnostic for Probabilistic Forecasting. arXiv preprint arXiv:2510.19110 <http://arxiv.org/abs/2510.19110>, 2025.

Gneiting, T. and Ranjan, R. Comparing density forecasts using threshold-and quantile-weighted scoring rules. *Journal of Business & Economic Statistics*, 29(3):411–422, 2011. ISSN 07350015. URL <http://www.jstor.org/stable/23243806>.

Gretton, A., Borgwardt, K. M., Rasch, M. J., Schölkopf, B., and Smola, A. A Kernel Two-Sample Test. *Journal of Machine Learning Research*, 13(25):723–773, 2012.

Hubert, M., Debruyne, M., and Rousseeuw, P. J. Minimum Covariance Determinant and Extensions. *WIREs Computational Statistics*, 10(3):e1421, 2018.

Kan, K., Aubet, F.-X., Januschowski, T., Park, Y., Benidis, K., Ruthotto, L., and Gasthaus, J. Multivariate Quantile Function Forecaster. In *Proceedings of The 25th International Conference on Artificial Intelligence and Statistics*, pp. 10603–10621, 2022.

Kiraly, F. J. and Oberhauser, H. Kernels for Sequentially Ordered Data. *Journal of Machine Learning Research*, 20(31):1–45, 2019.

Koochali, A., Schichtel, P., Dengel, A., and Ahmed, S. Random Noise vs. State-of-the-Art Probabilistic Forecasting Methods: A Case Study on CRPS-Sum Discrimination Ability. *Applied Sciences*, 12(10):5104, 2022.

Liu, C., Aksu, T., Liu, J., Liu, X., Yan, H., Pham, Q., Savarese, S., Sahoo, D., Xiong, C., and Li, J. Moirai 2.0: When Less Is More for Time Series Forecasting. arXiv preprint arXiv:2511.11698 <http://arxiv.org/abs/2511.11698>, 2025a.

Liu, G., Liu, J., Bai, Y., Wang, C., Wang, H., Zhao, H., Liang, G., Zhao, J., and Qiu, J. EWLD: A Large-Scale Industrial and Commercial Load Dataset in Extreme Weather Events. *Scientific Data*, 10(1):615, 2023.

Liu, X., Liu, J., Woo, G., Aksu, T., Liang, Y., Zimmermann, R., Liu, C., Li, J., Savarese, S., Xiong, C., and Sahoo, D. Moirai-MoE: Empowering Time Series Foundation Models with Sparse Mixture of Experts. In *Proceedings of the Forty-second International Conference on Machine Learning*, 2025b.

Liu, Y., Wu, H., Wang, J., and Long, M. Non-stationary Transformers: Exploring the Stationarity in Time Series Forecasting. In *Proceedings of the Thirty-Fifth Advances in Neural Information Processing Systems*, 2022.

Liu, Y., Hu, T., Zhang, H., Wu, H., Wang, S., Ma, L., and Long, M. iTransformer: Inverted Transformers Are Effective for Time Series Forecasting. In *Proceedings of the Twelfth International Conference on Learning Representations*, 2024.

Liu, Y., Qin, G., Shi, Z., Chen, Z., Yang, C., Huang, X., Wang, J., and Long, M. Sundial: A Family of Highly Capable Time Series Foundation Models. In *Proceedings of the Forty-second International Conference on Machine Learning*, 2025c.

Lyons, T. and McLeod, A. D. Signature Methods in Machine Learning. arXiv preprint arXiv:2206.14674 <http://arxiv.org/abs/2206.14674>, 2025.

Marcotte, É., Zantedeschi, V., Drouin, A., and Chapados, N. Regions of Reliability in the Evaluation of Multivariate Probabilistic Forecasts. In *Proceedings of the 40th International Conference on Machine Learning*, pp. 23958–24004, 2023.

Morrill, J., Fermanian, A., Kidger, P., and Lyons, T. A Generalised Signature Method for Multivariate Time Series Feature Extraction. arXiv preprint arXiv:2006.00873 <http://arxiv.org/abs/2006.00873>, 2021.

Nie, Y., Nguyen, N. H., Sinthong, P., and Kalagnanam, J. A Time Series is Worth 64 Words: Long-term Forecasting with Transformers. In *Proceedings of The Eleventh International Conference on Learning Representations*, 2023.

Rasul, K., Ashok, A., Williams, A. R., Ghonia, H., Bhagwatkar, R., Khorasani, A., Bayazi, M. J. D., Adamopoulos, G., Riachi, R., Hassen, N., Biloš, M., Garg, S., Schneider, A., Chapados, N., Drouin, A., Zantedeschi, V., Nevmyvaka, Y., and Rish, I. Lag-Llama: Towards Foundation Models for Probabilistic Time Series Forecasting. arXiv preprint arXiv:2310.08278 <http://arxiv.org/abs/2310.08278>, 2024.

Salinas, D., Bohlke-Schneider, M., Callot, L., Medico, R., and Gasthaus, J. High-dimensional multivariate forecasting with low-rank Gaussian Copula Processes. In *Proceedings of the Thirty-Second Conference on Advances in Neural Information Processing Systems*. Curran Associates, Inc., 2019.

Salvi, C., Cass, T., Foster, J., Lyons, T., and Yang, W. The Signature Kernel is the solution of a Goursat PDE. *SIAM Journal on Mathematics of Data Science*, 3(3):873–899, 2021.

Scheuerer, M. and Hamill, T. M. Variogram-Based Proper Scoring Rules for Probabilistic Forecasts of Multivariate Quantities. *Monthly Weather Review*, 143(4):1321–1334, 2015.

Shchur, O., Turkmen, A. C., Erickson, N., Shen, H., Shirkov, A., Hu, T., and Wang, B. Autogluon-timeseries: AutoML for probabilistic time series forecasting. In *AutoML Conference 2023 (ABCD Track)*, 2023. URL <https://openreview.net/forum?id=XHIY3cQ8Tew>.

Shchur, O., Ansari, A. F., Turkmen, C., Stella, L., Erickson, N., Guerron, P., Bohlke-Schneider, M., and Wang, Y. fev-bench: A Realistic Benchmark for Time Series Forecasting. arXiv preprint arXiv:2509.26468 <http://arxiv.org/abs/2509.26468>, 2025.

Wang, Y., Wu, H., Dong, J., Liu, Y., Wang, C., Long, M., and Wang, J. Deep Time Series Models: A Comprehensive Survey and Benchmark. arXiv preprint arXiv:2407.13278 <http://arxiv.org/abs/2407.13278>, 2025.

Woo, G., Liu, C., Kumar, A., Xiong, C., Savarese, S., and Sahoo, D. Unified Training of Universal Time Series Forecasting Transformers. In *Proceedings of the 41st International Conference on Machine Learning*, pp. 53140–53164, 2024.

Wu, H., Hu, T., Liu, Y., Zhou, H., Wang, J., and Long, M. TimesNet: Temporal 2D-Variation Modeling for General Time Series Analysis. In *Proceedings of The Eleventh International Conference on Learning Representations*, 2023.

Zawadzki, E. and Lahaie, S. Nonparametric Scoring Rules. In *Proceedings of the 29th AAAI Conference on Artificial Intelligence*, 2015.

Zeng, A., Chen, M., Zhang, L., and Xu, Q. Are transformers effective for time series forecasting? In *Proceedings of the 37th AAAI Conference on Artificial Intelligence*. AAAI Press, 2023.

Zhang, J., Wen, X., Zhang, Z., Zheng, S., Li, J., and Bian, J. ProbTS: Benchmarking Point and Distributional Forecasting across Diverse Prediction Horizons. In *Proceedings of the Thirty-Seventh Conference on Advances in Neural Information Processing Systems, Datasets and Benchmarks Track*, 2024.

A. Benchmark Results

Here we present the results of each model on each metric in the TSLib benchmarking datasets, results here include foundation models and learned forecasters.

Table 6. Benchmark results for the ETTh1 dataset.

Model	QL	CRPS	ES	VS	Sig	CSig
DLinear	0.1672	0.4204	1.3815	5.3419	0.6062	0.1636
NLinear	0.1749	0.4295	1.4048	5.4543	0.6131	0.1727
PatchTST	0.1592	0.4243	1.4140	4.9356	0.5976	0.1715
iTransformer	0.1791	0.4784	1.5619	5.8392	0.6938	0.1985
TimesNet	0.2024	0.4925	1.6610	6.0975	0.7897	0.2251
N-HiTS	0.1597	0.4155	1.3989	5.0582	0.6112	0.1771
NSTransformer	0.1947	0.4819	1.6083	5.8546	0.7152	0.1989
Naive Seasonal	0.2411	0.4258	1.4479	5.9381	0.8395	0.2038

Table 7. Benchmark results for the ETTh2 dataset.

Model	QL	CRPS	ES	VS	Sig	CSig
DLinear	0.1083	0.2823	0.9050	2.7828	0.1198	0.0739
NLinear	0.1120	0.2791	0.8996	2.7936	0.1212	0.0744
PatchTST	0.1049	0.2679	0.8859	2.6181	0.1150	0.0713
iTransformer	0.1228	0.3287	1.0517	3.5370	0.1394	0.0817
TimesNet	0.1777	0.4304	1.3960	4.6376	0.1637	0.1002
N-HiTS	0.1050	0.2826	0.9293	2.6492	0.1159	0.0714
NSTransformer	0.1249	0.3182	1.0589	3.2442	0.1372	0.0809
Naive Seasonal	0.1705	0.2846	0.9557	3.3525	0.2152	0.1282

Table 8. Benchmark results for the ETTm1 dataset.

Model	QL	CRPS	ES	VS	Sig	CSig
DLinear	0.1455	0.3622	1.2013	4.4639	0.2661	0.0682
NLinear	0.1521	0.3700	1.2195	4.4806	0.2676	0.0692
PatchTST	0.1477	0.3793	1.3205	4.6858	0.2754	0.0749
iTransformer	0.1618	0.4316	1.4217	5.1278	0.2916	0.0799
TimesNet	0.1869	0.4510	1.5407	5.7217	0.3117	0.0906
N-HiTS	0.1458	0.3741	1.2902	4.5421	0.2770	0.0742
NSTransformer	0.1870	0.4492	1.5360	5.6318	0.3020	0.0793
Naive Seasonal	0.3314	0.6064	2.0822	9.0746	0.4920	0.1250

Table 9. Benchmark results for the ETTm2 dataset.

Model	QL	CRPS	ES	VS	Sig	CSig
DLinear	0.0887	0.2252	0.7247	2.0916	0.0476	0.0378
NLinear	0.0902	0.2244	0.7238	2.1135	0.0484	0.0386
PatchTST	0.0859	0.2217	0.7263	1.9488	0.0461	0.0366
iTransformer	0.0925	0.2448	0.7861	2.1716	0.0487	0.0386
TimesNet	0.1106	0.2700	0.8810	2.6424	0.0589	0.0468
N-HiTS	0.0839	0.2203	0.7282	1.9945	0.0466	0.0371
NSTransformer	0.0980	0.2481	0.8175	2.3346	0.0512	0.0404
Naive Seasonal	0.1570	0.2577	0.8543	2.9558	0.0776	0.0598

Table 10. Benchmark results for the Weather dataset.

Model	QL	CRPS	ES	VS	Sig	CSig
DLinear	0.0955	0.2486	1.6729	34.2364	0.1439	0.0117
NLinear	0.0976	0.2561	1.6926	33.4748	0.1471	0.0117
PatchTST	0.0793	0.2068	1.5365	26.9961	0.1353	0.0118
iTransformer	0.0832	0.2155	1.5765	28.9550	0.1345	0.0116
TimesNet	0.0836	0.2089	1.5286	28.0194	0.1335	0.0118
N-HiTS	0.0754	0.1958	1.4923	26.3611	0.1316	0.0115
NSTransformer	0.0966	0.2358	1.7113	32.7672	0.1419	0.0120
Naive Seasonal	0.1464	0.2364	1.7032	37.8302	0.1739	0.0124

Table 11. Benchmark results for the Exchange Rate dataset.

Model	QL	CRPS	ES	VS	Sig	CSig
DLinear	0.0760	0.2042	0.6947	1.4686	0.0855	0.0427
NLinear	0.0764	0.1979	0.6791	1.4745	0.0982	0.0524
PatchTST	0.1074	0.2907	1.0381	3.7299	0.0978	0.0473
iTransformer	0.1637	0.3920	1.4031	9.3085	0.1350	0.0689
TimesNet	0.3173	0.6804	2.3758	14.9033	0.1740	0.0801
N-HiTS	0.0900	0.2473	0.8223	1.5759	0.1003	0.0482
NSTransformer	0.1169	0.2738	0.9555	2.4166	0.1198	0.0541
Naive Seasonal	0.1412	0.2261	0.8004	2.3363	0.1011	0.0498

Table 12. Benchmark results for the Illness dataset.

Model	QL	CRPS	ES	VS	Sig	CSig
DLinear	0.5383	1.0768	3.2927	11.9622	1.2493	0.6940
NLinear	0.4621	0.9592	2.9975	10.2003	1.0770	0.6297
PatchTST	0.6160	1.3112	4.1198	21.4009	1.2695	0.7444
iTransformer	0.6019	1.2872	4.1639	23.5057	1.1910	0.6905
TimesNet	0.7744	1.5814	5.0090	21.1246	1.3151	0.7613
N-HiTS	0.5966	1.2246	3.8218	14.1085	1.2513	0.6953
NSTransformer	0.4647	1.1098	3.3790	8.0747	1.1567	0.6561
Naive Seasonal	1.1700	2.2835	6.8269	15.6432	1.9478	0.9392

Signature-Kernel Based Evaluation Metrics

Table 13. Probabilistic Foundation Model Results ETTh1

Model	QL	CRPS	ES	VS	Sig	CSig
Chronos-2	0.1392	0.4061	1.3772	4.767614	0.566930	0.129741
Moirai	0.1694	0.3399	1.1563	6.901941	0.825062	0.127911
MoiraiMoE	0.1660	0.3309	1.1306	7.030968	0.825239	0.125499

Table 14. Probabilistic Foundation Model Results ETTh2

Model	QL	CRPS	ES	VS	Sig	CSig
Chronos-2	0.0926	0.2684	0.9061	2.621097	0.082572	0.044752
Moirai	0.1030	0.2073	0.7035	3.024887	0.196999	0.085248
MoiraiMoE	0.1013	0.2037	0.6912	2.960636	0.165252	0.073267

Table 15. Probabilistic Foundation Model Results ETTm1

Model	QL	CRPS	ES	VS	Sig	CSig
Chronos-2	0.1155	0.3279	1.1292	3.793850	0.235547	0.052119
Moirai	0.2048	0.4093	1.4396	8.877374	0.883098	0.100518
MoiraiMoE	0.1942	0.3811	1.3948	10.719838	0.907058	0.098285

Table 16. Probabilistic Foundation Model Results ETTm2

Model	QL	CRPS	ES	VS	Sig	CSig
Chronos-2	0.0727	0.2060	0.6939	1.843815	0.039654	0.028553
Moirai	0.0961	0.1922	0.6570	2.918322	0.231770	0.131532
MoiraiMoE	0.1098	0.1873	0.6559	1669.427425	0.255027	0.149303

Table 17. Probabilistic Foundation Model Results Weather

Model	QL	CRPS	ES	VS	Sig	CSig
Chronos-2	0.0607	0.1695	1.4041	23.346514	0.120584	0.013371
Moirai	9.1758	0.1611	1.2272	22995.516708	0.541872	0.025575
MoiraiMoE	30.7473	0.1847	1.8027	77459.324710	0.867537	0.034001

Table 18. Probabilistic Foundation Model Results Exchange Rate

Model	QL	CRPS	ES	VS	Sig	CSig
Chronos-2	0.0674	0.1976	0.6997	1.476679	0.105833	0.001284
Moirai	0.0821	0.1644	0.5907	1.965205	0.291127	0.001120
MoiraiMoE	0.0800	0.1594	0.5790	1.999032	0.298691	0.001155

Table 19. Probabilistic Foundation Model Results Illness

Model	QL	CRPS	ES	VS	Sig	CSig
Chronos-2	0.2159	0.5961	1.9114	4.689043	0.829515	0.364208
Moirai	0.4085	0.8172	2.5250	9.220842	1.055205	0.320231
MoiraiMoE	0.3305	0.6631	2.2081	9.370012	1.033853	0.317864

B. Extreme Weather Event Results

Here we present the results of learned and foundation model forecasters on our extreme weather event datasets.

Table 20. Benchmark results for the EWELD dataset.

Model	QL	CRPS	ES	VS	Sig	CSig
DLinear	0.2078	0.4807	2.9398	72.5962	1.0969	0.0471
NLinear	0.1874	0.4731	2.8132	62.1465	1.0064	0.0454
PatchTST	0.1567	0.4206	2.8122	52.2024	1.0003	0.0465
iTransformer	0.1657	0.4416	2.8391	60.5918	1.0217	0.0471
TimesNet	0.1693	0.4290	2.8566	55.1992	1.0051	0.0475
N-HiTS	0.1563	0.4250	2.8300	53.3105	0.9999	0.0463
NSTransformer	0.1724	0.4530	2.9816	54.6870	1.0127	0.0474
Naive Seasonal	0.2746	0.4928	3.1262	66.2851	1.3920	0.0510

Table 21. Benchmark results for the ERA5 dataset.

Model	QL	CRPS	ES	VS	Sig	CSig
DLinear	0.1177	0.2763	1.8035	31.5393	0.5065	0.0794
NLinear	0.1194	0.2778	1.8153	31.3250	0.5110	0.0790
PatchTST	0.0952	0.2467	1.7826	23.9394	0.4563	0.0782
iTransformer	0.0893	0.2333	1.7015	22.2972	0.4290	0.0766
TimesNet	0.0896	0.2247	1.6377	22.1337	0.4107	0.0771
N-HiTS	0.0900	0.2317	1.7389	23.3082	0.4450	0.0770
NSTransformer	0.0945	0.2383	1.7801	23.9477	0.4451	0.0776
Naive Seasonal	0.1750	0.2936	2.0266	35.5818	0.6511	0.0865

Table 22. Probabilistic Foundation Model Results EWELD

Model	QL	CRPS	ES	VS	Sig	CSig
Chronos-2	0.1401	0.4143	2.8056	51.41	0.994720	0.038768
Moirai	91.1496	0.3399	2.4835	30.98×10^5	1.078215	0.027276
MoiraiMoE	22.1465	0.3176	2.1390	43.45×10^3	1.070205	0.027120

Table 23. Probabilistic Foundation Model Results ERA5 Land

Model	QL	CRPS	ES	VS	Sig	CSig
Chronos-2	0.0867	0.2452	1.8725	24.60	0.464560	0.090050
Moirai	37.7260	0.1993	1.4684	55.51×10^3	0.791564	0.071203
MoiraiMoE	2.5778	0.1998	1.4322	14.67×10^2	0.811589	0.071214

C. Regions of Reliability

To provide further insight into the usage of our metric and appropriate sample sizes we conduct four hypothesis testing experiments. The heat-maps generated for each experiment are shown below.

Following the methodology of the Regions of Reliability framework, we evaluate the statistical power of our metrics—*SigMMD* and *Censored SigMMD (CSigMMD)*—across varying problem dimensionalities ($d \in \{8, 16, 32, 64\}$) and forecast sample sizes ($m \in \{64, 128, 256, 512\}$). Statistical power measures the true positive rate: the ability of a scoring rule to correctly identify a known discrepancy between a ground-truth distribution and an erroneous forecast at a fixed significance level ($\alpha = 0.05$). The discrepancy parameters for each scenario were adopted from the ROR benchmark codebase to ensure that the detection task remains calibrated to an 80% power baseline, with regards to the predictive power of negative log likelihood) across all dimensionalities.

Wrong Mean (All Dimensions). This experiment tests a basic failure where the forecast distribution is shifted in mean across all dimensions relative to the ground truth. As seen in Figure 4, both metrics exhibit high reliability for larger sample sizes, but power typically drops as the dimensionality d increases relative to m , demonstrating the expected challenge where more samples are required to maintain discriminative power in high dimensions.

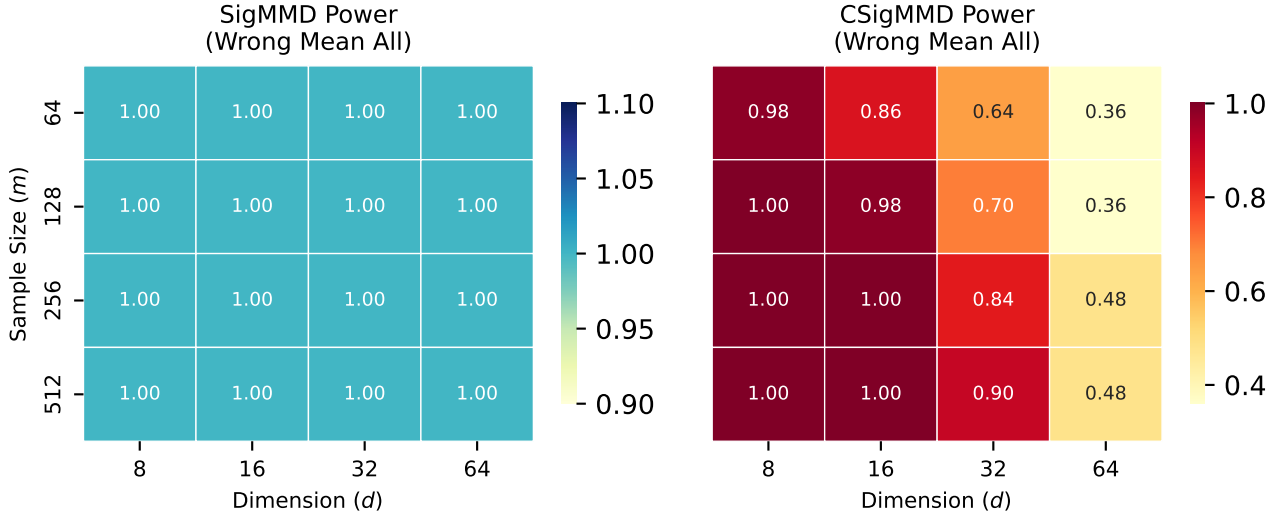


Figure 4. Power heatmaps for Wrong Mean (All Dimensions) experiment.

Wrong Exponential Scaling (All Dimensions). We evaluate the metrics’ sensitivity to scale errors by using an Exponential distribution where the forecast has a higher mean, and thus higher variance, than the ground truth. Figure 5 illustrates the region of reliability where signature-based metrics successfully distinguish between different scaling factors.

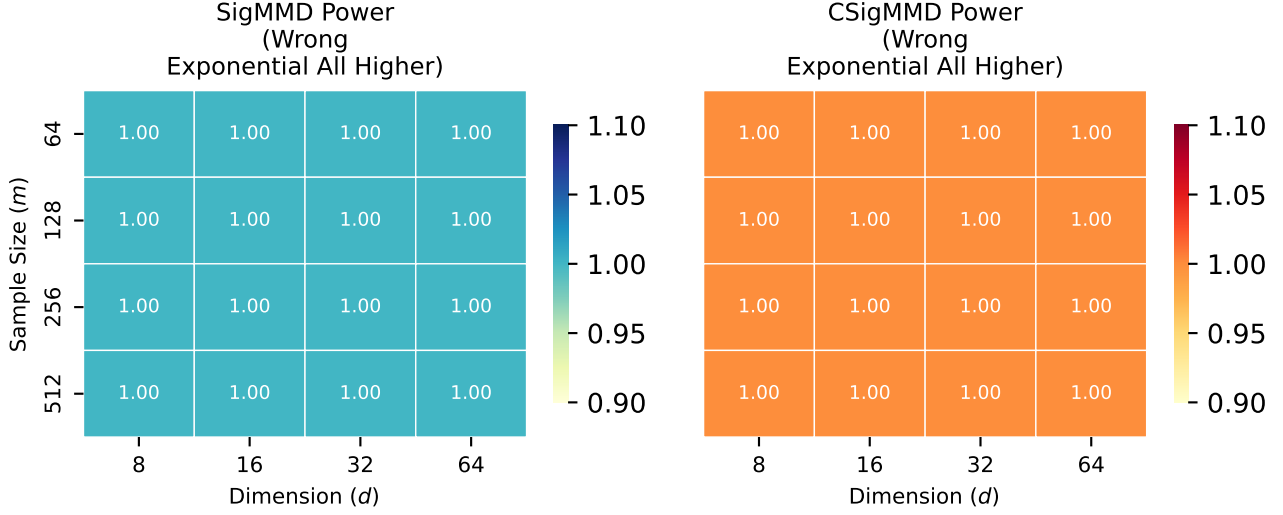


Figure 5. Power heatmaps for Wrong Exponential Scaling experiment.

Missing Skewness (All Dimensions). In this case, the ground truth is a skewed distribution, while the forecast is a symmetric Normal distribution with matching mean and covariance. This tests whether the signature-based metrics can capture higher-order moments that standard scoring rules often fail to detect.

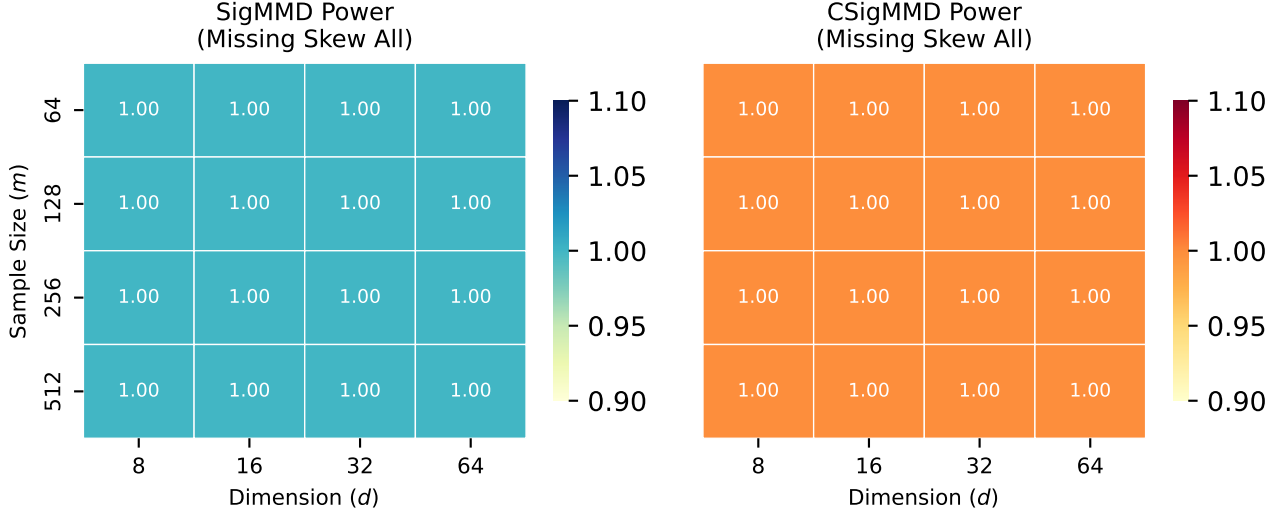


Figure 6. Power heatmaps for Missing Skewness experiment.

Missing Full Covariance. This experiment measures the ability to detect a complete lack of correlation structure in the forecast when the ground truth contains positive correlations. These results highlight the specific sample regimes where our metrics remain reliable for dependency detection. The weak performance of CSig on this metric is due to H_1 being relatively stable so as not to introduce tails, and the ground truth Gaussian also not having large tails, thus at the sample sizes tested there are no points in the censored region causing the metric to default to 0. If the censored region increases it is shown in 3 that CSig will converge towards Sig, thus increasing statistical power on these scenarios. This highlights an important point that for stable data with thin tails the censoring quantile should be reduced as we have done with weather in our benchmarks.

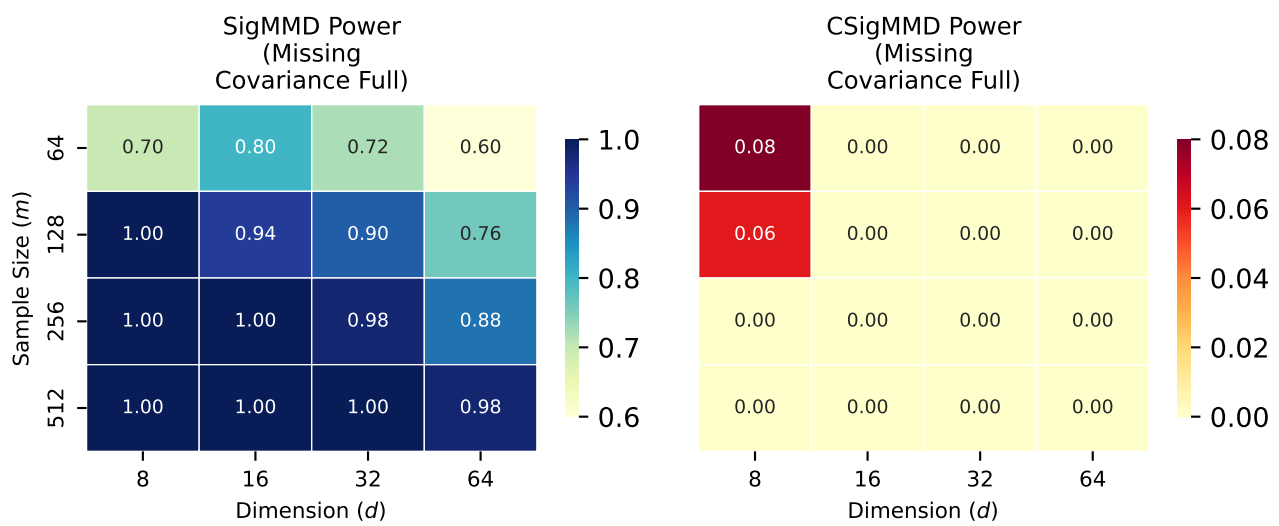


Figure 7. Power heatmaps for Missing Full Covariance experiment.

D. Kernel Choice Ablation

Here we ablate the kernel choice on our synthetic distribution experiments to examine the difference between a standard RBF MMD, Sig-MMD, and CSig-MMD, the experiments here follow the same experimental setup as Sec. 5.2:

Table 24. Dependency Experiment: F_1 the forecaster outputs samples from the ground truth distribution, F_2 the forecaster outputs samples from the ground truth without temporal correlations, F_3 the forecaster outputs samples from the ground truth without spatial and temporal correlations, and F_4 the forecaster outputs samples from the ground truth with Bernoulli arrival jumps. This table shows that MMD also maintains properness as expected but lacks the sensitivity to correlation changes shown in our proposed signature based metrics.

F	MMD	Sig	CSig
F_1	0.000708	0.000733	0.000051
F_2	0.000901	0.009174	0.000078
F_3	0.000925	0.010376	0.000082
F_4	0.008772	0.002757	0.000239

Table 25. Focus Experiment: F_1 the forecaster outputs the ground truth, F_2 paths from the body of the distribution have harmonic noise added, F_3 the forecaster samples from a t-distribution, F_4 the forecaster samples from a uniform distribution. This table shows that MMD is even less sensitive to tails than the signature-kernel MMD likely due to the better geometric representation provided by the signature transformation, this also reiterates that both metrics are unable to differentiate quality of tail forecasts as capably as our censored Sig-MMD

F	MMD	Sig	CSig
F_1	0.000000	0.000000	0.000000
F_2	0.154538	0.158023	0.000000
F_3	0.103297	0.229519	0.000203
F_4	0.003763	0.058396	0.000153

The results here clearly demonstrate the improvements provided by our signature based metrics and censoring process when compared to MMD with a standard RBF kernel.

E. ERA-5 Setup

The variates chosen for ERA-5 are made up of various different variate types, including:

- **Atmospheric Pressure**

- *sp*: Surface Pressure (pressure at the Earth's surface)
- *tp*: Total Precipitation

- **Heat Radiation**

- *ssrd*: Surface Solar Radiation Downwards (Shortwave radiation)
- *strd*: Surface Thermal Radiation Downwards (Longwave radiation)

- **Surface & Snow**

- *skt*: Skin Temperature (temperature of the surface interface)
- *snowc*: Snow Cover (fractional snow cover on the grid)

- **Soil Temperature (4 Layers)**

- *stl1*: Soil Temperature Level 1 (0–7 cm)
- *stl2*: Soil Temperature Level 2 (7–28 cm)
- *stl3*: Soil Temperature Level 3 (28–100 cm)
- *stl4*: Soil Temperature Level 4 (100–289 cm)

- **Soil Water Level (4 Layers)**

- *swvl1*: Volumetric Soil Water Layer 1 (0–7 cm)
- *swvl2*: Volumetric Soil Water Layer 2 (7–28 cm)
- *swvl3*: Volumetric Soil Water Layer 3 (28–100 cm)
- *swvl4*: Volumetric Soil Water Layer 4 (100–289 cm)

- **Near-Surface Temperature**

- *d2m*: 2m Dewpoint Temperature
- *t2m*: 2m Air Temperature

- **Wind Level (10m Vectors)**

- *u10*: 10m U-component of Wind (Eastward)
- *v10*: 10m V-component of Wind (Northward)